# Self-Penetration—A Structural Compromise between Single Networks and Interpenetration: Magnetic Properties and Crystal Structures of $[Mn(dca)_2(H_2O)]$ and $[M(dca)(tcm)]$, M = Co, Ni, Cu, dca = Dicyanamide, $N(CN)_2^-$, tcm = Tricyanomethanide, $C(CN)_3^-$

**Paul Jensen, David J. Price, Stuart R. Batten, Boujemaa Moubaraki, and Keith S. Murray*[a]**

*Dedicated to the memory of Professor Olivier Kahn*

**Abstract:** The three-dimensional coordination polymers $[Mn(dca)_2(H_2O)]$ (**1**) and $[M(dca)(tcm)]$, M = Co (**2**), Ni (**3**), Cu (**4**), dca = dicyanamide, $N(CN)_2^-$, tcm = tricyanomethanide, $C(CN)_3^-$, have isomorphous structures. In **1** half the dca ligands coordinate directly (through all three nitrogen atoms) to three Mn atoms (all metal atoms are six-coordinate), while the other half coordinate to two Mn atoms (through the nitrile nitrogens) and hydrogen bond to water molecules coordinated to a third Mn atom (through the amide nitrogen). This $dca \cdot H_2O$ structural moiety is disordered over a mirror plane, and is replaced by the structurally equivalent tcm ligand in compounds **2**–**4**. The resulting structures display a new self-penetrating 3,6-connected (2:1) network topology that can be related to, but is different from, the rutile net. The self-penetrating $[M(dca)(tcm)]$ network can be viewed as a structural compromise between the two interpenetrating rutile-like networks of $[M(tcm)_2]$ and the single rutile-like network of $\alpha$-$[M(dca)_2]$. The temperature and field dependence of the DC and AC magnetic susceptibilities and magnetisations has been measured for complexes **1**–**4**. Compounds **1**–**3** exhibit long-range magnetic order with critical temperatures of 6.3 K for **1**, 3.5 K for **2** and 8.0 K for **3**. The $Cu^{II}$ compound **4** does not order and is essentially a paramagnet. Hysteresis measurements of coercive field and remnant magnetisation show that **1**, **2** and **3** are soft magnets, **1** being a canted-spin antiferromagnet (weak ferromagnet), while **2** and **3** are ferromagnets that display some unusual features in their high-field magnetisation isotherms in comparison to their related $\alpha$-$[M(dca)_2]$ phases.

**Keywords:** coordination chemistry · crystal engineering · dicyanamide · magnetic properties · tricyanomethanide

## Introduction

Entangled systems are of great chemical interest due to the interesting topological and physical properties displayed by such systems. Molecular entanglement, in the form of catenanes, rotaxanes and knots is well known.[1] Entanglement of ordered polymeric networks, that is, *interpenetration*, is also of great current interest, and numerous well-characterised systems are known.[2] Interpenetration occurs when two or more unconnected infinite networks pass through each other such that they cannot be separated without breaking of bonds within the networks. They are polymeric equivalents of catenanes and rotaxanes.

The polymeric equivalent of a molecular knot is a *self-penetrating* (*self-entangled* or *intra*penetrating) network. These networks are single networks that nonetheless contain regions in which rods pass through rings in a similar fashion to interpenetrating systems. While rods and rings in any network can be chosen such that a rod passes through a ring, a useful and necessary restriction is to define a network as self-penetrating only when the *smallest topological circuits* are penetrated by rods.[3, 4] A smallest circuit is defined as the minimum number of nodes it takes to leave a chosen node along one link and return to the starting node through a different link. The smallest topological circuits are not necessarily all the same size.

[a] Prof. K. S. Murray, P. Jensen, D. J. Price, Dr. S. R. Batten, Dr. B. Moubaraki
Department of Chemistry, P.O. Box 23
Monash University 3800 (Australia)
Fax: (+61) 3-9905-4597
E-mail: keith.s.murray@sci.monash.edu.au

  0947-6539/00/0617-3186 $ 17.50+.50/0 

We report here four new compounds that possess a new self-penetrating network topology. Three of the compounds also show long-range magnetic ordering, which is related to their unusual structures. The structures arise from our ongoing interest in the structural and magnetic properties of coordination polymers containing the pseudohalide ligands tricyanomethanide (tcm, $C(CN)_3^-$) and dicyanamide (dca, $N(CN)_2^-$). The compounds $[M(tcm)_2]$, $M^{II}$ = Cr, Mn, Fe, Co, Ni, Cu, Zn, Cd and Hg, contain two interpenetrating rutile-related networks.[2, 5] Similarly, the compounds $\alpha$-$[M(dca)_2]$, $M^{II}$ = Cr, Mn, Fe, Co, Ni and Cu, also contain rutile-related networks, although in this case no interpenetration occurs.[6] Although investigation of the magnetic properties of $[M(tcm)_2]$ uncovered only weak coupling and no long-range ordering, the magnetic properties of $\alpha$-$[M(dca)_2]$ were much more varied and interesting, ranging from long-range ferromagnetism (Co, Ni) to spin-canted antiferromagnetism (Mn, Fe) to simple paramagnetism (Cu).

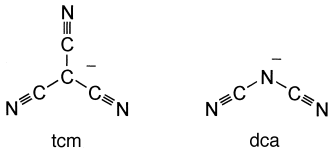


A number of other coordination polymers containing either tcm[2, 5c, 7] or dca[6b–d, 8] have also been crystallographically characterised by different teams. In particular, we have already reported the formation of two products obtained from the reaction of $Mn^{II}$ and dca in water—$\alpha$-$[Mn(dca)_2]$, which has a single rutile-like network, and $[Mn(dca)_2(H_2O)_2]\cdot H_2O$, which contains linear chains penetrating (4,4) sheets.[6b, 6d] We report here the structure and magnetism of a third product, namely $[Mn(dca)_2(H_2O)]$ (**1**), and of $[M(dca)(tcm)]$, M = Co (**2**), Ni (**3**) and Cu (**4**). They all contain the same self-penetrating network structure. Indeed, although **1** was obtained fortuitously, compounds **2**–**4** were the result of a deliberate crystal-engineering strategy based on the structure of **1**. We have also found that **1** is responsible for a magnetic transition noted[6d] weakly at 6 K in the magnetisation versus temperature plot of the parent $[Mn(dca)_2]$, a spin-canted antiferromagnet with $T_N = 16$ K. The hydrate was present as a trace impurity. The compounds **2** and **3** are new homometallic long-range-ordered magnets, while **4** is essentially a paramagnet.

## Results and Discussion

**Synthesis and crystal structures:** Crystals of **1** were obtained by slow evaporation of either solutions of $[Mn(dca)_2]$ in wet methanol/ethanol, or of aqueous solutions of $Mn(ClO_4)_2\cdot 6H_2O$ and Na(dca). Unlike $[Mn(dca)_2(H_2O)_2]\cdot H_2O$, compound **1** appears not to lose solvent at room temperature upon removal from the mother liquor. The structure of **1** was solved by X-ray crystallography (Table 1).

The structure contains octahedral Mn atoms coordinated to (on average) five dca ligands and one water ligand. The dca ligands are of two types—one coordinates to three Mn atoms through each of the three nitrogen atoms (dca1), while the other coordinates directly to two Mn atoms through the nitrile nitrogens only (dca2). The dca2 ligands also form hydrogen bonds through the amide nitrogens to the water molecules, which are also coordinated to the Mn atoms. This $dca2\cdot H_2O$ moiety, however, is disordered over two positions which are related by a mirror plane. While the amide nitrogen and one of the nitrile groups of dca2 (and the Mn atom coordinated to this nitrile) lie on the mirror plane, the other nitrile group and the water ligand do not. In fact they have symmetry-related positions that superimpose on each other, with the affected nitrogen and oxygen atoms given the same positional parameters. Consequently the O···N hydrogen-bonding distance is constrained to be the same as the NCN distance within the dca2 ligand (O1···N4 = 2.633(7) Å), and the position of the disordered carbon is the only site without full occupancy by a non-hydrogen atom. The result of this disorder is the creation of a trigonal moiety within the

Table 1. Selected crystallographic and data collection parameters for compounds **1**–**4**.

| | $[Mn(dca)_2(H_2O)]$ (**1**) | $[Co(dca)(tcm)]$ (**2**) | $[Ni(dca)(tcm)]$ (**3**)[a] | $[Cu(dca)(tcm)]$ (**4**) | |
|---|---|---|---|---|---|
| formula | $MnC_4N_6H_2O$ | $CoC_6N_6$ | $NiC_6N_6$ | $CuC_6N_6$ | |
| $M_r$ | 205.06 | 215.05 | 214.83 | 219.66 | |
| crystal system | orthorhombic | orthorhombic | orthorhombic | orthorhombic | orthorhombic |
| space group | *Ama*2 (no. 40) | *Ama*2 (no. 40) | *Ama*2 (no. 40) | *Ama*2 (no. 40) | *Ama*2 (no. 40) |
| $a$ [Å] | 7.5743(2) | 7.4129(3) | 7.309(2) | 7.2041(3) | 7.1884(3) |
| $b$ [Å] | 17.4533(7) | 17.0895(6) | 16.999(6) | 17.4837(6) | 17.6983(7) |
| $c$ [Å] | 5.6353(2) | 5.5991(2) | 5.562(2) | 5.7281(2) | 5.7395(3) |
| $V$ [Å$^3$] | 744.97(4) | 709.31(5) | 691.0(3) | 721.48(5) | 730.19(6) |
| $Z$ | 4 | 4 | 4 | 4 | 4 |
| $T$ [K] | 293(2) | 173(2) | 295(1) | 123(2) | 297(2) |
| $\rho_{calcd}$ [g cm$^{-3}$] | 1.83 | 2.014 | 2.065 | 2.022 | 1.998 |
| $\mu$ [cm$^{-1}$] | 17.28 | 23.67 | | 29.75 | 29.40 |
| $F(000)$ | 404 | 420 | | 428 | |
| $2^\circ\ \theta_{max}$ [°] | 60.06 | 55.68 | 64.64 | 60.06 | |
| $hkl$ ranges | $0 \le h \le 9$ | $-9 \le h \le 9$ | | $-10 \le h \le 10$ | $-10 \le h \le 10$ |
| | $-24 \le k \le 0$ | $-22 \le k \le 22$ | | $-22 \le k \le 23$ | $-23 \le k \le 24$ |
| | $0 \le l \le 7$ | $-6 \le l \le 6$ | | $-8 \le l \le 8$ | $-8 \le l \le 8$ |
| data collected | 5465 | 5006 | | 5272 | 5276 |
| unique data ($R_{int}$) | 611 (0.037) | 888 (0.044) | | 1115 (0.045) | 1126 (0.045) |
| observed data [$I > 2\sigma(I)$] | 554 | 856 | | 1076 | 1055 |
| parameters | 68 | 66 | | | 66 |
| final $R_1$, $wR_2$ [$I > 2\sigma(I)$][b] | 0.0262, 0.0571 | 0.0228, 0.0528 | | 0.0240, 0.0585 | 0.0253, 0.0543 |
| $R_1$, $wR_2$ (all data) | 0.0333, 0.0615 | 0.0244, 0.0534 | | 0.0259. 0.0593 | 0.0297, 0.0554 |
| weighting scheme ($a$, $b$)[b] | 0.0184, 0.7932 | 0.0155, 1.5132 | | 0.0276, 1.0625 | 0.0191, 0.7086 |
| goodness of fit | 1.199 | 1.108 | | 1.115 | 1.148 |
| Flack parameter | 0.62(12) | 0.01(3) | | 0.01(2) | 0.00(2) |
| $\Delta\rho_{min}$, $\Delta\rho_{max}$ [e Å$^{-3}$] | 0.53, −0.38 | 0.36, −0.33 | | 0.42, −0.45 | 0.36, −0.38 |

[a] From X-ray powder diffraction ($\lambda = 1.54059$ Å) at 295 K. [b] $R_1 = \Sigma\,|\,\Delta F\,|\,/\Sigma\,|\,F_o\,|$, $wR_2 = [\Sigma[w(F_o^2 - F_c^2)^2]/\Sigma w(F_o^2)^2]^{1/2}$ in which $w^{-1} = [\sigma^2(F_o^2) + (aP)^2 + bP]$ and $P = [F_o^2 + 2F_c^2]/3$.

  0947-6539/00/0617-3187 $ 17.50+.50/0 

structure, as shown in Figure 1. A more informative formula for the structure would thus be [Mn(dca1)(dca2·$H_2O$)]. Selected bond lengths and angles are given in Table 2.

The disordered dca2·$H_2O$ moiety was recognised to be geometrically very similar to the tcm anion (Figure 1), so we attempted to engineer new materials which had the same network, but with tcm replacing the disordered dca2·$H_2O$ moiety. Half of the dca in the reaction mixture was replaced with tcm, and crystalline products were obtained for Co, Ni and Cu. X-ray crystallography showed the new products, [M(dca)(tcm)], M = Co (**2**), Ni (**3**) and Cu (**4**), did indeed have the desired topology (while useable single crystals were not obtained for **3**, powder X-ray diffraction was used to show it was isomorphous with **1**, **2** and **4**). In fact, they possess the same space group and similar cell parameters (Table 1) as **1**. Bond lengths and angles are given in Table 3. The network topology is perhaps explained more easily for [M(dca)(tcm)], and in comparison to the rutile networks of [M(dca)$_2$] (1 net) and [M(tcm)$_2$] (2 nets). Both structures, however, have the same topology and thus the description of [M(dca)(tcm)] applies equally as well for **1**.

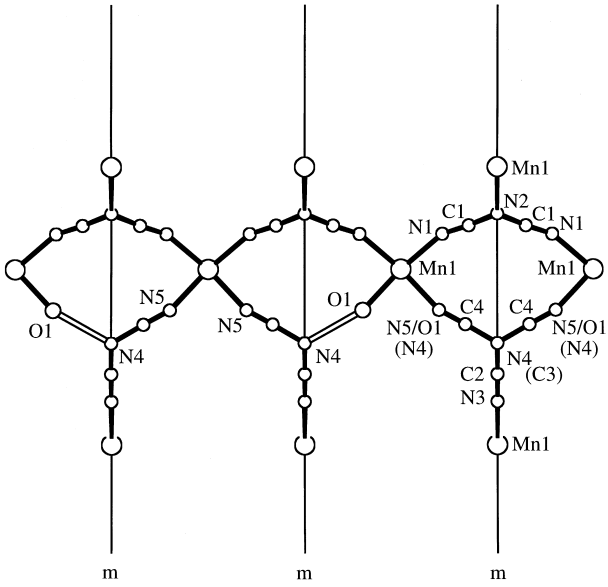


Figure 1. A chain in the structure of [Mn(dca)$_2$($H_2O$)] (**1**) showing the disorder of the dca2·$H_2O$ system over the mirror plane (thin line). The two different orientations of the system are shown (left and middle) as well as the resultant sum of the disorder (right). The hydrogen bond is denoted by the open bond, and the atom numbering scheme for [M(dca)(tcm)] (where different to **1**) is shown in brackets. Symmetry related atoms are not distinguished.

Table 2. Selected interatomic distances [Å] and angles [°] for **1**.[a]

| | | | |
|---|---|---|---|
| Mn1–N1 | 2.191(4) | Mn1–N3 | 2.171(5) |
| Mn1–N5$^{I}$ | 2.190(4) | Mn1–O1$^{I}$ | 2.190(4) |
| Mn1–N2$^{II}$ | 2.417(4) | N1–C1 | 1.148(4) |
| C1–N2 | 1.307(4) | N3–C2 | 1.146(7) |
| C2–N4 | 1.325(8) | N4–C3 | 1.460(7) |
| N5–C3 | 1.175(6) | O1···N4 | 2.633(7) |
| N3-Mn1-N1 | 94.8(2) | N3-Mn1-N1$^{III}$ | 94.8(2) |
| N3-Mn1-N5$^{I}$ | 96.5(1) | N1-Mn1-N5$^{I}$ | 87.7(1) |
| N1-Mn1-N5$^{IV}$ | 167.7(2) | N1-Mn1-N1$^{III}$ | 95.9(2) |
| N3-Mn1-N2$^{II}$ | 178.7(3) | N1-Mn1-N2$^{II}$ | 178.7(3) |
| N1-Mn1-N2$^{II}$ | 84.3(1) | C1-N1-Mn1 | 157.3(4) |
| C1-N2-C1$^{V}$ | 118.3(4) | C1-N2-Mn1$^{VI}$ | 120.6(2) |
| C2-N3-Mn1 | 162.9(5) | C2-N4-C3 | 118.0(3) |
| C3-N4-C3$^{III}$ | 119.2(7) | C3-N5-Mn1$^{VII}$ | 161.7(4) |
| N1-C1-N2 | 174.5(4) | N3-C2-N4 | 178.4(6) |
| N5-C3-N4 | 176.2(6) | | |

[a] Symmetry transformations: I: $-x, -y, z-1$; II: $-x, 1/2-y, z-1/2$; III: $1/2-x, y, z$; IV: $x+1/2, -y, z-1$; V: $-x-1/2, y, z$; VI: $-x, 1/2-y, z+1/2$; VII: $-x, -y, z+1$.

Table 3. Bond lengths [Å] and angles [°] for **2** and **4**.[a]

| | **2** | **4**[b] | **4**[c] |
|---|---|---|---|
| M1–N1 | 2.099(2) | 1.983(2) | 1.980(2) |
| M1–N4$^{I}$ | 2.101(2) | 1.992(2) | 1.989(2) |
| M1–N3 | 2.122(3) | 2.360(3) | 2.390(3) |
| M1–N2$^{VI}$ | 2.192(3) | 2.526(3) | 2.564(3) |
| N1–C1 | 1.152(3) | 1.150(3) | 1.142(3) |
| C1–N2 | 1.319(3) | 1.307(3) | 1.305(3) |
| N3–C2 | 1.182(6) | 1.188(6) | 1.197(6) |
| C2–C3 | 1.464(6) | 1.461(6) | 1.460(6) |
| C3–C4 | 1.390(3) | 1.378(3) | 1.377(3) |
| C4–N4 | 1.147(3) | 1.148(3) | 1.141(3) |
| N1-M1-N3 | 92.59(9) | 94.07(9) | 94.0(1) |
| N1-M1-N1$^{II}$ | 95.7(1) | 93.0(1) | 93.0(1) |
| N1-M1-N4$^{I}$ | 84.63(8) | 86.90(8) | 86.90(8) |
| N1-M1-N4$^{III}$ | 174.97(9) | 174.21(9) | 174.2(1) |
| N1-M1-N2$^{VI}$ | 86.31(8) | 86.2(1) | 85.7(1) |
| N3-M1-N4$^{I}$ | 92.41(9) | 91.72(9) | 91.83(9) |
| N3-M1-N2$^{VI}$ | 178.4(1) | 180.0(1) | 180.0(1) |
| N4$^{I}$-M1-N4$^{III}$ | 94.7(1) | 92.6(1) | 92.6(1) |
| N4$^{I}$-M1-N2$^{VI}$ | 88.70(8) | 88.1(1) | 88.5(1) |
| C1-N1-M1 | 158.4(2) | 155.8(2) | 155.6(2) |
| N1-C1-N2 | 175.9(3) | 175.0(3) | 174.6(3) |
| C1-N2-C1$^{IV}$ | 117.3(3) | 119.0(3) | 119.2(3) |
| C1-N2-M1$^{VII}$ | 121.3(2) | 120.5(4) | 120.4(4) |
| C2-N3-M1 | 158.9(4) | 150.1(3) | 152.2(4) |
| N3-C2-C3 | 178.4(5) | 177.8(4) | 178.3(5) |
| C2-C3-C4 | 120.7(2) | 120.8(2) | 120.8(2) |
| C4-C3-C4$^{II}$ | 117.3(3) | 117.8(3) | 117.9(3) |
| C3-C4-N4 | 179.5(3) | 179.8(3) | 179.8(3) |
| C4-N4-M1$^{V}$ | 169.1(2) | 167.5(2) | 167.5(2) |

[a] Symmetry transformations: I: $-x, -y, z-1$; II: $1/2-x, y, z$; III: $x+1/2, -y, z-1$; IV: $-x-1/2, y, z$; V: $-x, -y, z+1$; VI: $-x, 1/2-y, z-1/2$; VII: $-x, 1/2-y, z+1/2$. [b] 123 K. [c] 297 K.

As implied above, the structure is closely related to the rutile network. Network topology is an important consideration in the design, construction, analysis and exploitation of new, ordered, polymeric networks (whether coordination polymers or hydrogen-bonded networks), and the rutile network (Figure 2a) is one of the important basic networks that result from the combination of three-connecting and six-connecting centres (in the ratio 2:1).[9]

The rutile structure ($TiO_2$; octahedral Ti, trigonal O) can be described in terms of square channels in which the three-connecting centres form the sides of the channels, and the six-connecting centres occupy the corners (Figure 2a). These channels can be constructed by cross-linking $TiO_2$ chains arranged such that adjacent chains are perpendicular (Figure 2a). The sides of these channels contain six-membered rings (alternating three- and six-connecting centres), which are the second smallest rings within the structure. The smallest are four-membered rings within the afore-mentioned chains,

  0947-6539/00/0617-3188 $ 17.50+.50/0 *Chem. Eur. J.* **2000**, *6*, No. 17

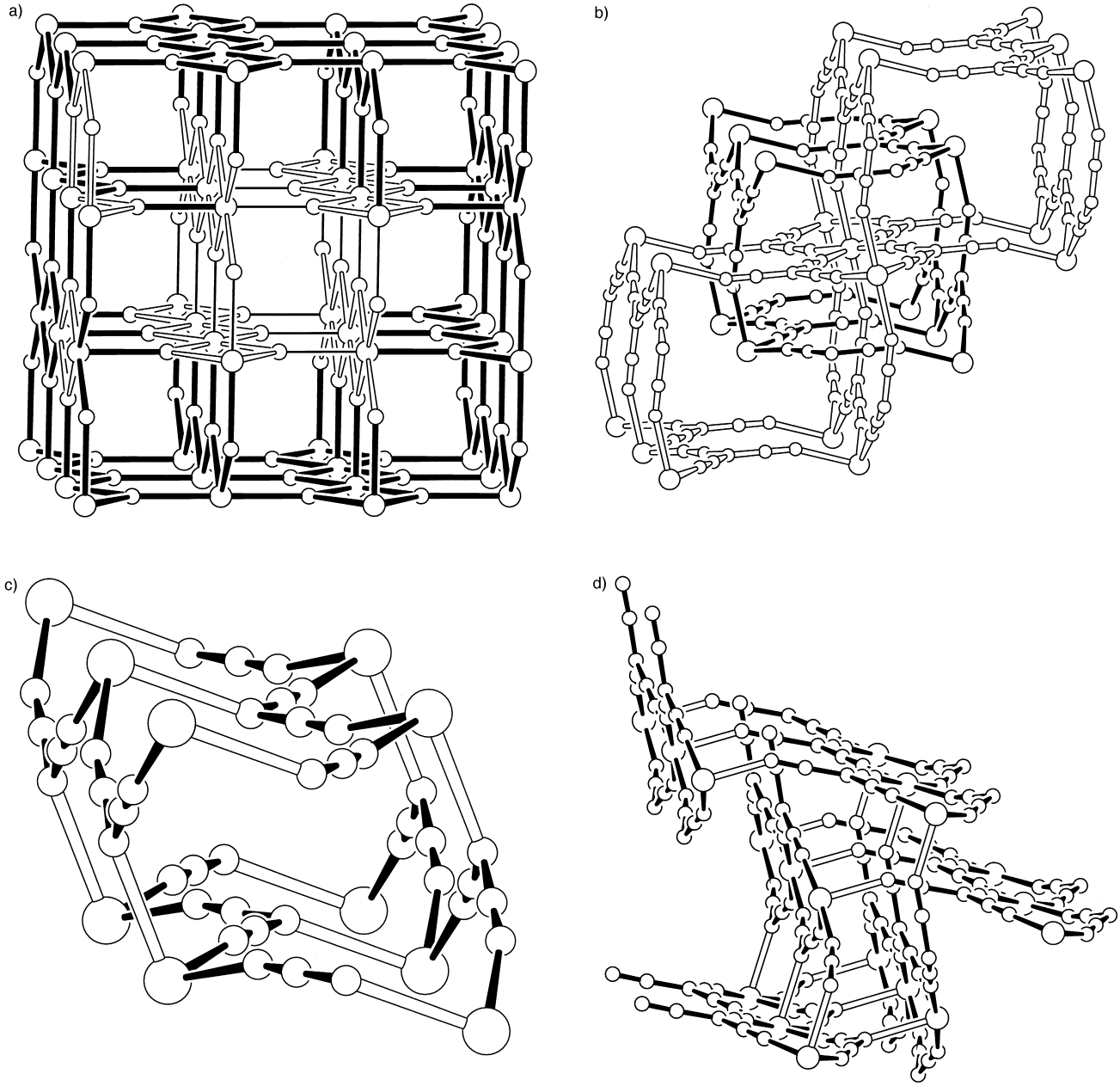


Figure 2. The rutile ($TiO_2$) framework. Octahedral centres (Ti) are represented by large circles and trigonal centres (O) are represented by small circles. A square channel is highlighted in the centre by the open bonds (the four separate chains) and the thin bonds (the connections between the chains which give the channel). A four-membered ring (left) and a six-membered ring (top left) are also highlighted by open bonds. b) A square channel in the rutile-like structure of $[M(tcm)_2]$ interpenetrated by a second identical network. c) A square channel in the rutile-like structure of $\alpha$-$[M(dca)_2]$. The $M{-}N_{amide}$ connections between the four perpendicular chains which generate the channel are highlighted by the open bonds. d) The connection of four perpendicular chains in the structure of [M(dca)(tcm)]. The interchain connections are highlighted by the open bonds. Compare the result to the square channels generated in $[M(tcm)_2]$ and $\alpha$-$[M(dca)_2]$. All figures are viewed from equivalent angles.

which also contain alternating three- and six-connecting centres. Both the four- and six-membered rings are, however, "smallest circuits" in a topological sense.

In the $[M(tcm)_2]$ structures, the distance between the octahedral centres and the trigonal centres is large (ca. 4.5–5.0 Å), and thus a porous network results. This allows the interpenetration of a second network. The interpenetration is such that rods of one network pass through the six-membered rings (from a topological point of view—i.e., only the nodes are counted) of the second network (Figure 2b). The four-membered rings are too small to sterically allow penetration of a rod from the second network.

In the rutile-like structure of $[M(dca)_2]$, while two-thirds of the trigonal to octahedral node distances are similar to those in $[M(tcm)_2]$, one-third are considerably shorter ($M{-}N_{amide}$ vs. M-NC-C). This results in a considerably denser, less spacious rutile network, which does not allow interpenetration. Structurally, the bonds which are shorter are the bonds *between* the chains that form the square channels (Figure 2c). This means that the sizes of the four-membered rings are not affected, but

  0947-6539/00/0617-3189 $ 17.50+.50/0 

the six-membered rings, through which the rods of the second network pass in the interpenetrating $[M(tcm)_2]$ structures, are considerably smaller. Too small, it appears, to allow penetration, and thus interpenetration does not occur.

In the structure of [M(dca)(tcm)], we combine the three long links of tcm and the one short/two long links of dca. In this structure the short dca link again occurs *between* the $ML_2$ chains. If we examine the connections between four adjacent chains analogous to those which form the square channels in the two previous rutile-like structures, the similarities and differences of the new network to rutile become apparent. The chains, all of which are crystallographically equivalent, have the formula [M(dca)(tcm)] and have tcm ligands on one side of the chain and dca ligands on the other. Again, adjoining chains are mutually inclined to each other, and are connected by the third link of the three-connecting centres joining to the axial positions of the six-connecting metal centres. The requirement that the M···M distance within the chains must be the same for the dca bridge as for the tcm bridge means that the metal to amide nitrogen link of the dca must be the *interchain* bond. This means, however, that the interchain linkages of the three-connecting centres to the six-connecting centres are of different lengths, depending on whether the ligand is tcm or dca. In other words, in this structure we have two types of trigonal nodes—one with three long links of equal length (tcm) and one with two long links and one short link (dca). The structural consequences of this are shown in Figure 2d. The first two interchain linkages are of the long tcm type. The second two linkages between chains, however, are of the short dca type. Therefore, while the four chains in rutile connect to form a square channel, the network of interconnected chains in [M(dca)(tcm)] falls short of returning to its starting point, and folds back through itself in the spiral fashion shown in Figure 2d. As for $[M(tcm)_2]$, the penetration occurs such that the six-membered $M_3(tcm)_3$ rings are penetrated by C-CN-M rods of the tcm anions. In this case, however, it is a single network penetrating itself. Penetration does not occur through the four-membered rings or the smaller $M_3(dca)_3$ six-membered rings.

In summary, we find that if we combine octahedral metal ions with a ligand with three long links (tcm) we get two interpenetrating rutile-like networks, while combination of octahedral metals with a ligand that contains one short and two long links (dca) results in a single rutile-like network. If, however, we use *both* ligands, we get a structural compromise between the two parent structures—a single, self-penetrating network with a topology different but closely related to rutile.

A schematic view of the overall network is shown in Figure 3. We mentioned previously the importance of smallest circuits in the topology of a network for defining a self-penetrating network. The total number of smallest circuits from any given *p*-connected node in a network (which is simply equal to the number of possible combinations of any two links radiating from the node) is equal to $p(p-1)/2$. The value is halved so that each circuit is only counted once. To illustrate, inspection of the rutile network (Figure 2a) reveals that there are 15 smallest circuits that start from a six-connecting centre ($p=6$): two $fou_5r$-membered, ten six-membered and three eight-membered rings. The smallest

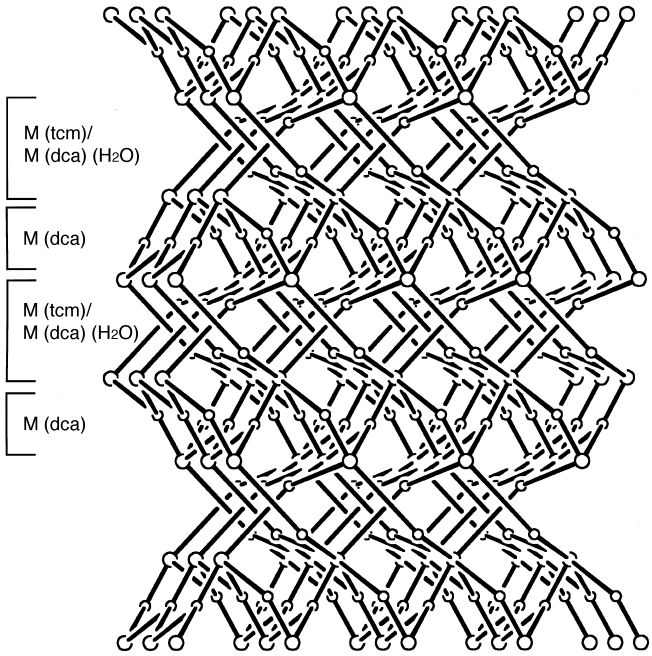


Figure 3. A schematic view of the [M(dca)(tcm)] network, with only the octahedral and trigonal centres shown. Layers of M(tcm) [or M(dca)-($H_2O$)] and M(dca) in the structure are highlighted (see text).

circuits starting from the three-connecting centres ($p=3$) are one four-membered and two six-membered rings. In the self-penetrating network (Figure 3), the distribution and size of the smallest rings are the same as rutile: four-, six- and eight-membered rings (2:10:3) for the six-connecting nodes, and four- and six-membered rings (1:2) for each of the two types of three-connecting centres. Thus although they have different topologies, rutile and [M(dca)(tcm)] have the same Schläfli notation: $(4^2 6^{10} 8^3)(4^1 6^2)$.

As mentioned above, in the interpenetrating rutile networks of $[M(tcm)_2]$ the penetration occurs through the six-membered rings, which are a "smallest circuit" of the rutile network. Similarly, the penetration in the [M(dca)(tcm)] network also occurs through the six-membered "smallest circuits". Thus we can describe the network as *self-penetrating*. Recently a number of other self-penetrating networks have been reported.[3, 4, 10] The structure also represents a new network topology for 3,6-connected networks with the connectors in the ratio 2:1. Previously described topologies include the above-mentioned rutile[5, 6, 9] and $[Hg(tpt)_2(ClO_4)_2]\cdot 6\,C_2H_2Cl_4$.[11]

The close similarity of the tcm and $dca\cdot H_2O$ structural moieties also resulted in the structures of **2**–**4** being doped by small random amounts of $dca\cdot H_2O$ (in place of tcm). The IR spectra contained sharp $H_2O$ bending frequencies at 1618 (**2**), 1616 (**3**) and 1619 $cm^{-1}$ (**4**), and the elemental analyses showed the presence of small amounts of hydrogen. In each structure the thermal parameters for one of the tcm carbon atoms (C2; the only atom not replaced by a similar non-hydrogen atom when tcm is replaced by $dca\cdot H_2O$ is a nitrile carbon) were higher than most of the other atoms in the structures. This last fact, along with analysis of the powder X-ray diffraction pattern (which showed that the only other



0947-6539/00/0617-3190 $ 17.50+.50/0 *Chem. Eur. J.* **2000**, *6*, No. 17

phase present is $[M(tcm)_2]$—the analysis was also consistent with some $[M(tcm)_2]$ impurities), leads us to believe that the water is present as a doping in the crystal structure of the tcm moiety by the $dca \cdot H_2O$ moiety, rather than as separate phases of [M(dca)(tcm)] and $[M(dca)_2(H_2O)]$. In addition, no evidence of $[M(dca)_2(H_2O)]$ was seen in the magnetism or powder X-ray diffraction of samples of $[M(dca)_2]$ previously prepared from water for M = Co, Ni or Cu,[6a] unlike M = Mn, as discussed elsewhere. This indicates that tcm, although it is partially replaced by $dca \cdot H_2O$, is still an essential component in the Co, Ni and Cu structures.

**Magnetic properties:** Complex **1** is another example of the growing number of homometallic spin-canted antiferromagnets (weak ferromagnets).[6b, 6d, 6h, 12–16] In a field of 0.3 T this high spin $d^5$ species shows a $\mu_{Mn}$ value at 300 K of 5.64 $\mu_B$ ($\chi T = 3.98\ cm^3 mol^{-1} K$). As the temperature is decreased the $\mu_{Mn}$ values gradually decrease due to antiferromagnetic coupling, reaching 2.62 $\mu_B$ ($\chi T = 0.86\ cm^3 mol^{-1} K$) at 4.2 K (Figure 4). The Weiss constant from the $\chi$ versus $1/T$ plot is

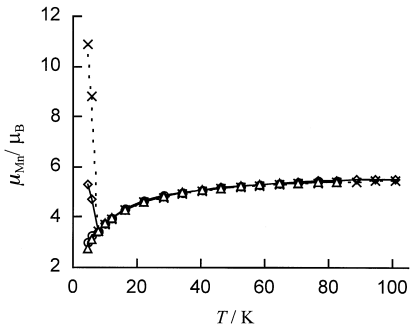


Figure 4. Plots of magnetic moment, $\mu_{Mn}$, versus temperature in various applied fields for **1**. Field values 20 Oe (×), 200 Oe (◇), 1000 Oe (○), 3000 Oe (△). (Note that the $\chi_{Mn}T$ values can be obtained from $\mu_{Mn}^2 = 7.997\chi_{Mn}T$)

−4.2 K. In field values below about 200 Oe the magnetic moments show an abrupt increase at approximately 6 K due to the occurence of long-range order. Thus $\mu_{Mn}$ is 10.9 $\mu_B$ at 4.2 K in a field of 20 Oe. The $T_N$ value of 6.3 K was confirmed by measuring the magnetisation ($M$) values in zero-field-cooled (ZFCM) and field-cooled (FCM, 5 Oe) modes (Figure 5). The $\chi'$ versus $T$ plot of the AC in-phase susceptibility

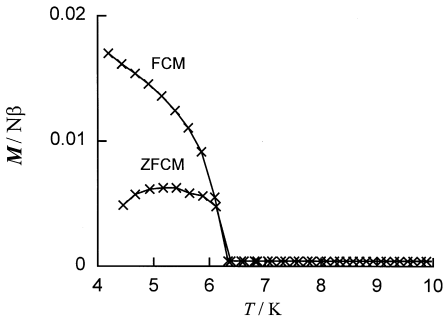


Figure 5. Plots of magnetisation, $M$, versus temperature for **1** measured with zero-field cooling (ZFCM) and field cooling (FCM; DC field = 5 Oe).

showed a very sharp maximum at 6.3 K typical of a weak ferromagnet. Hysteresis measurements on a neat powder at 2 K showed a remnant magnetisation (RM) of 112 $cm^3 mol^{-1}$ Oe and coercive field of 250 Oe, values typical of a soft magnet (Figure 6). High-field magnetisation data, with tem-

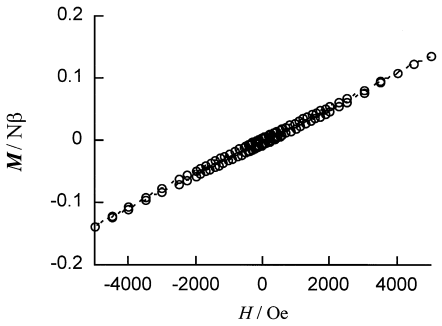


Figure 6. Hysteresis loop for **1** measured on a powder sample at 2 K.

peratures above and below the ordering temperature, again show evidence for spin-canted antiferromagnetism in terms of linear behaviour and low values of $M$ at the highest field used, for example, 1.7 Nβ at 5 T and 2 K ($M_{sat}$ for $Mn^{II}$ would be 5 Nβ).

The key structural features of **1** that give rise to the antiferromagnetic coupling are the three-connecting dca and $dca \cdot H_2O$ bridges, dominated by the chains of $Mn^{II}$ ions bridged through the nitrile nitrogen atoms, as in the cases of $[Mn(dca)_2]$ and $[Mn(dca)_2L_2]$ chain systems.[6b, 6d, 6f] Use of Rushbrooke and Wood theory[17] for the coupling of $S = 5/2$ centres led to a best fit set of parameters of the 0.3 T susceptibility data of $g = 1.93$ and $J = -0.19\ cm^{-1}$, agreement below 30 K being poor. The $J$ value is similar to those in the $[Mn(dca)_2L_2]$ series.[6b, 6d]

The occurrence of long-range spin-canting arises through a combination of bridging through the amide nitrogen atom and, importantly, the disposition of adjacent Mn chromophores at 60.6° to each other along the $N_{amide}$-bridged pathways. This appears to be a common structural feature in other recent molecule-based examples of spin-canting.[12, 14, 15] Self-penetration of the polymeric network does not appear to lead to any interactions between chains.

The mixed ligand, high-spin complexes [M(dca)(tcm)], M = Co (**2**) and Ni (**3**), display long-range order at $T_c$ values of 3.5 K and 8.0 K, respectively, temperatures that are approximately one-third of those displayed by the $[M(dca)_2]$ parents.[6a, 6e, 6h] The magnetic moment data for **3** in a field of 1 T are shown in Figure 7. The $\mu_{Ni}$ value at 300 K of 3.05 $\mu_B$ ($\chi T = 1.16\ cm^3 mol^{-1} K$) shows a small but gradual increase as the temperature is decreased, typical of ferromagnetic coupling, with a rapid increase to a maximum of 5.39 $\mu_B$ at 7.9 K, followed by a rapid decrease to 3.02 $\mu_B$ at 2 K. The Weiss constant for susceptibility is +4.9 K over the temperature range 4–300 K. In smaller applied fields the rise to a sharp maximum becomes more abrupt such that in a field of 200 Oe the $\mu_{max}$ value is 23 $\mu_B$ ($\chi T = 66.1\ cm^3 mol^{-1} K$). Such behaviour is typical of the occurence of a magnetic phase transition. Confirmation is provided in Figure 8, which shows

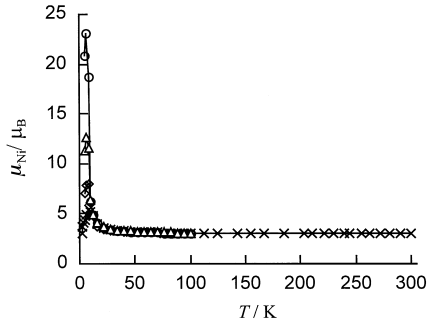


Figure 7. Plots of $\mu_{Ni}$ versus temperature for **3** in applied fields of 10000 Oe (×), 3000 Oe (◇), 2000 Oe (△), 200 Oe (○).

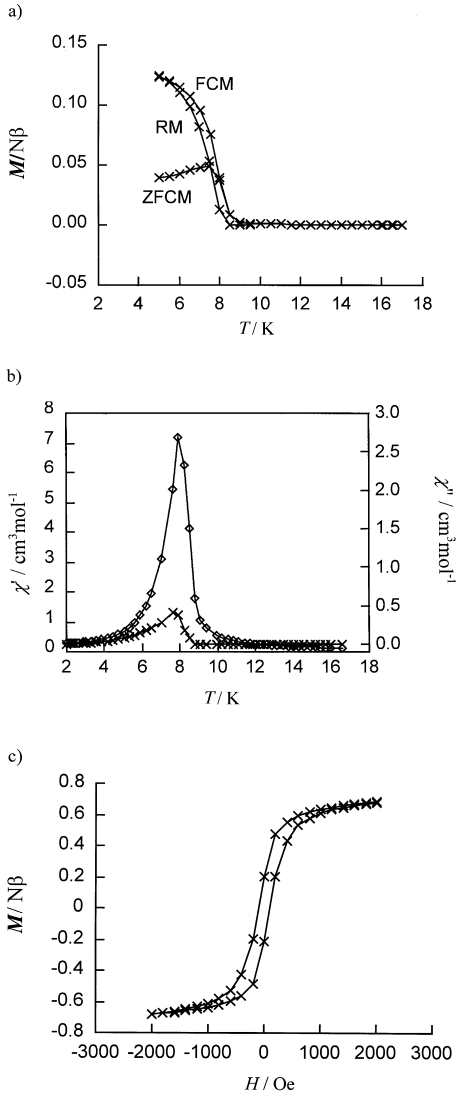


Figure 8. a) Plots of FCM, ZFCM and RM (remnant magnetisation) for **3** using a field of 5 Oe. b) Plots of in-phase (◇) and out-of-phase (×) AC susceptibilities of **3** versus temperature in a field of 3.5 Oe oscillating at 20 Hz. c) Hysteresis loop for **3** measured as a powder at 5 K.

plots of FCM, ZFCM and RM in a DC field of 5 Oe, a hysteresis loop at 5 K in fields of ±2000 Oe and the in-phase and out-of-phase components of AC susceptibilities, the in-phase plot showing a maximum at $T_c$. The RM is 1151 $cm^3 mol^{-1}$ Oe and the coercive field is 100 Oe, which can be compared with those for $[Ni(dca)_2]$ of 5027 $cm^3 mol^{-1}$ Oe and 220 Oe (at 5 K; dependent on temperature and particle size[6a, 6e, 6h, 18]). The high-field $\boldsymbol{M}$ versus $H$ plots measured at temperatures between 2 and 20 K show differences in detail when compared with those of the ferromagnet $[Ni(dca)_2]$,[6a, 6e, 6h] particularly below $T_c$. Thus, at 2 K, after a very rapid, almost spontaneous, increase in $\boldsymbol{M}$ at low fields, as anticipated for a ferromagnet, the $\boldsymbol{M}$ values then slowly increase and do not saturate below a field of 5 T, being 1.75 Nβ at 5 T. This may be due to a competing antiferromagnetic ordering, also responsible for the decrease in $\boldsymbol{\mu}_{eff}$ which occurs at very low temperatures below $\boldsymbol{\mu}_{max}$. It may also be due to spin-canting as in **1**, but the shape of the $\chi'$ peak in the AC data of Figure 8 is much more ferromagnetic-like.

DC and AC measurements show that **2** orders at 3.5 K. In Figure 9 it can be seen that the $\boldsymbol{\mu}_{Co}$ versus temperature plot in

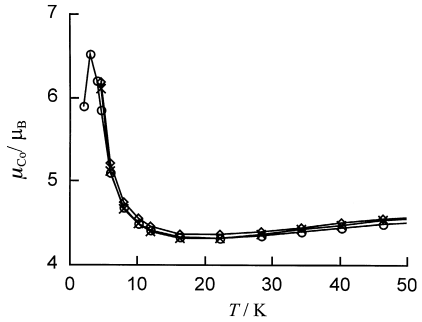


Figure 9. Plots of $\boldsymbol{\mu}_{Co}$ versus temperature (2 to 100 K) for **2** in applied fields of 3000 Oe (◇), 1000 Oe (×), 200 Oe (○). Not shown here are the 20 Oe data, which rise abruptly to a maximum of 21.95 $\mu_B$ at very low temperatures.

a DC field of 0.3 T shows a moment at 290 K of 5.20 $\mu_B$ ($\chi T$ = 3.39 $cm^3 mol^{-1}$ K), which decreases very gradually to reach a broad minimum of 4.32 $\mu_B$ at 22 K, reminiscent of ferrimagnetic behaviour but possibly due mainly to single-ion spin-orbit splitting combined with ferromagnetic order.[5c] In a field of 200 Oe, the moment reaches a sharp maximum of 6.51 $\mu_B$ before decreasing to reach 5.89 $\mu_B$ at 4.2 K. In smaller applied fields such as 20 Oe (not shown) the moments increase sharply below temperatures of 10 K, due to long-range order, such that a value of 21.95 $\mu_B$ is observed at a sharp maximum at 3 K. Similarly shaped $\boldsymbol{\mu}_{Co}$ versus temperature curves have recently been observed for other octahedral $Co^{II}$ systems.[19, 20] The ordering temperature is confirmed by measurements of ZFCM and FCM (5 Oe DC field) and a $\chi'$ maximum in the AC susceptibilities (Figure 10). The hysteresis loop measured at 2.5 K between ±1000 Oe has an RM value of 186 $cm^3 mol^{-1}$ Oe and coercive field of 17 Oe, indicative of a very soft magnet with values much reduced from those in the ferromagnet $[Co(dca)_2]$.[6a, 6e, 6h] Plots of $\boldsymbol{M}$ versus $H$ at temperatures above and below the ordering temperature are shown in Figure 11. At 2 K, the $\boldsymbol{M}$ values increase very rapidly in very low fields on account of ordering, then begin to saturate above 2 T reaching 2.1 $\mu_B$ at 5 T, a value well below the $S = 3/2$ $\boldsymbol{M}_{sat}$ value of 3 Nβ. Similarly reduced values were observed in $[Co(dca)_2]$ and $[Co(tcm)_2]$ (not ordered) and are due primarily

  0947-6539/00/0617-3192 $ 17.50+.50/0 *Chem. Eur. J.* **2000**, *6*, No. 17

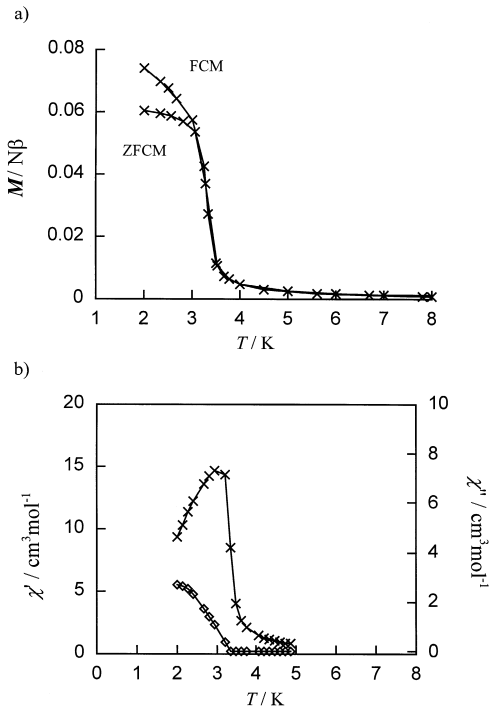


Figure 10. a) FCM (DC field of 5 Oe) and ZFCM data for **2**. b) In-phase, $\chi'$ (×), and out-of-phase, $\chi''$ (◇), AC susceptibilities for **2** in a field of 3.5 Oe oscillating at 20 Hz.

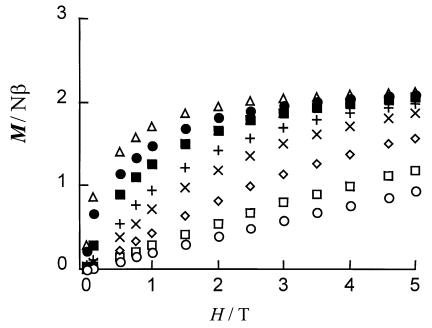


Figure 11. Magnetisation isotherms for **2** measured at 2 K (△), 3 K (●), 4 K (■), 5.5 K (+), 7 K (×), 10 K (◇), 15 K (□), 20 K (○).

to spin-orbit coupling effects within the $^4T_{1g}$ single ion states.[5c, 6a, 6e, 6h] The shapes of the $\boldsymbol{M}/H$ plots are quite unlike those of a recently reported canted-spin antiferromagnet ($T_N = 9$ K), $[Co(HCONH_2)_2(HCO_2)_2]$,[12b] in which the $\boldsymbol{M}$ values increase approximately linearly with $H$, do not saturate and are of the order of 0.66 Nβ at $H = 5.5$ T and 2 K. The [Co(dca)(tcm)] complex is much more weakly antiferromagnetically coupled, if at all, than is the formate example. Consideration of all the magnetic data for [Co(dca)(tcm)], including the ferromagnetic-like shape of the AC $\chi'$ versus $T$ plot, would suggest that spin-canting is not important.

A plot of $\boldsymbol{\mu}_{eff}$ versus temperature for [Cu(dca)(tcm)], in an applied field of 1 T, is Curie-like over the whole range ($\boldsymbol{\mu}_{eff} = 1.76\ \mu_B$), except for a very small increase in $\boldsymbol{\mu}_{eff}$ evident at low temperatures. This is reminiscent of the behaviour reported for a sample of $[Cu(dca)_2]$ prepared from ethanol.[6h] The present compound does not show any long-range order, most likely due to the Jahn–Teller lengthening of the $Cu-N_{amide}$ bond (Table 3).

We have noted above that these [M(dca)(tcm)] compounds consist of a single-phase material plus traces of a separate $[M(tcm)_2]$ phase. The single phase is effectively $[M(dca)(tcm)_x(dca \cdot H_2O)_{1-x}]$, in which tcm is randomly replaced with small quantities of $dca \cdot H_2O$. The magnetic studies have clearly shown that the bulk samples of **2** and **3** display a single, well-defined magnetic phase transition. The traces of $[M(tcm)_2]$ present in the samples will not influence the long-range order since the $[M(tcm)_2]$ compounds are not ordered.[5c] While we believe that the [M(dca)(tcm)] host is responsible for the observed long-range order, it is possible that neat samples of this and of $[M(dca)(dca \cdot H_2O)]$ would behave similarly magnetically and have near-identical powder X-ray diffraction patterns. Work is in progress to obtain such undoped single phases for M = Mn, Fe, Co, Ni and Cu, the monohydrate of Mn (**1**) being described here.

Finally, it is of interest to look at an alternative view of the three-dimensional networks of **1**–**4** to try to explain the magnetic features. Parallel two-dimensional zig-zag (6,3) sheets of M(dca) can be distinguished within the network (Figure 3), which alternate with layers that contain two interpenetrating M(tcm) (or $M(dca \cdot H_2O)$) (6,3) sheets which give rise to the self-penetration. Within the M(dca) sheets the tridentate dca bridges will dominate the exchange coupling and lead to long-range order (except for Cu), as observed in the parent $\alpha$-$[M(dca)_2]$ rutile-like phases. The anionic linking groups between the sheets will give rise to weaker coupling. In separate work, we are investigating structure–magnetism relations in complexes of the type $[R_4E][M(dca)_3]$, E = As, P, N, in which two-dimensional sheets are separated by $R_4E^+$ organic cations of different sizes.[21] Day et al.[22] have recently noted the sensitivity of the type of long-range order and the size of $T_c$ in the $[R_4E][M^{II}M^{III}(C_2O_4)_3]$ sheet structures to the nature of the $R_4E^+$ cation used.

## Experimental Section

**Synthesis of 1**

*Method A*: $[Mn(dca)_2]$[6d] (30 mg, 0.16 mmol) was dissolved in of hot methanol (5 mL). On cooling to room temperature ethanol (5 mL) was added. Crystals of **1** suitable for X-ray diffraction were afforded by slow evaporation of this solution over a period of several months. The majority of the crystals were triangular in habit and insensitive to solvent loss. IR (Nujol): $\tilde{\nu}$ = 3611, 3577, 3521, 3389, 3113, 2310, 2258, 2185, 1626, 1359, 1326, 955, 937, 679, 668 $cm^{-1}$; elemental analysis calcd (%) for $C_4H_2MnN_6O$ (205.06): C 23.4, N 41.0, H 1.0; found: C 23.6, N 41.3, H 0.8.

*Method B*: Aqueous solutions (5 mL each) of $Mn(ClO_4)_2 \cdot 6H_2O$ (362 mg, 1.0 mmol) and Na(dca) (178 mg, 2.0 mmol) were combined. Slow evaporation over two weeks yielded several aggregates of crystals and a small number of mainly irregularly shaped single crystals (some of which were of triangular habit) that were filtered and washed with ethanol. Yield: 82 mg (40 %); IR (Nujol): $\tilde{\nu}$ = 3520, 3222, 3111, 2309, 2257, 2183, 1625, 1359, 1324, 1057, 1006, 956, 938, 681, 667 $cm^{-1}$; elemental analysis calcd (%) for $C_4H_2MnN_6O$ (205.06): C 23.4, N 41.0, H 1.0; found: C 23.5, N 41.4, H 0.8. The powder X-ray diffraction pattern matched that calculated from the crystal structure data.

**Synthesis of 2:** A hot solution (6 mL) of $Co(NO_3)_2 \cdot 6H_2O$ (390 mg, 1.34 mmol) was added to a hot aqueous solution (6 mL) of Na(dca) (100 mg, 1.12 mmol) and K(tcm) (145 mg, 1.12 mmol). The resulting solution was allowed to cool and a pink/red microcrystalline product formed over several days. The product was filtered and washed with water. Yield: 150 mg (62 %); IR (Nujol): $\tilde{\nu}$ = 3462, 2295, 2282, 2264, 2215sh, 2197,

1618, 1357, 1314, 1268, 1253, 1070, 966 $cm^{-1}$; elemental analysis calcd (%) for $CoC_6N_6$ (215.05): C 33.51, N 39.09, H 0.00; found: C 33.99, N 37.73, H 0.25. The analytical figures are indicative of the presence of small amounts of $dca \cdot H_2O$ in place of tcm. Powder X-ray diffraction also showed the presence of traces of $[Co(tcm)_2]$. Single crystals were grown by layering an aqueous solution of $Co(NO_3)_2 \cdot 6H_2O$ and Na(dca) with $H_2O$, MeOH, then a solution of $(Me_4N)$(tcm) in MeOH. Small pink crystals formed after several days.

**Synthesis of 3:** A hot aqueous solution (3 mL) of $Ni(NO_3)_2 \cdot 6H_2O$ (408 mg, 1.40 mmol) was added to a hot aqueous solution (3 mL) of Na(dca) (100 mg, 1.12 mmol) and K(tcm) (147 mg, 1.14 mmol). The resulting solution was allowed to cool and a blue microcrystalline product formed over several days. The product was filtered and washed with water. Yield: 210 mg (87 %); IR (Nujol): $\tilde{\nu} = 3589, 3456, 2330, 2304, 2290, 2270, 2212, 1616, 1316, 1268, 1254, 1088, 972\ cm^{-1}$; elemental analysis calcd (%) for $NiC_6N_6$ (214.83): C 33.54, N 39.13, H 0.00; found: C 32.12, N 37.59, H 0.40. As in **2**, these figures are indicative of the presence of small amounts of $dca \cdot H_2O$ in place of tcm. Powder X-ray diffraction also showed the presence of traces of $[Ni(tcm)_2]$.

**Synthesis of 4:** A hot aqueous solution (6 mL) of $Cu(NO_3)_2 \cdot 3H_2O$ (288 mg, 1.19 mmol) was added to a hot aqueous solution (6 mL) of Na(dca) (100 mg, 1.12 mmol) and K(tcm) (145 mg, 1.12 mmol). The resulting solution was allowed to cool and a green/brown crystalline product formed over several days. The product was filtered and washed with water. Yield: 195 mg (79 %); IR (Nujol): $\tilde{\nu} = 3620, 3482, 2332, 2271, 2206, 2181$ (sh), 1619, 1360, 1259, 1088, 964 $cm^{-1}$; elemental analysis calcd (%) for $CuC_6N_6$ (219.66): C 32.79, N 38.26, H 0.00; found: C 30.54, N 38.30, H 0.29. As in **2** and **3**, these figures are indicative of the presence of small amounts of $dca \cdot H_2O$ in place of tcm.

**Crystallography:** Crystal data and details of the structure determinations are presented in Table 1. Data were collected on a Nonius KappaCCD diffractometer with graphite monochromated $Mo_{K\alpha}$ radiation ($\lambda =$ 0.71073 Å), using $\phi$ and $\omega$ rotations with 1° frames. The images were processed with the HKL suite of programs.[23] Data for **4** were collected at two different temperatures (123 and 297 K). Absorption corrections (face-indexed) were applied only to the data for **4**, at both temperatures (min./max. transmission factors = 0.717/0.862 (123 K), 0.721/0.863 (297 K)). Solutions were obtained by using either SHELXS-97[24] or teXsan[25] followed by successive difference Fourier transform methods, and structures were refined against $F^2$ using SHELXL-97.[24] The absolute configurations of **2** and **4** were assigned on the basis of the Flack parameter (Table 1), while **1** was refined as a racemic twin. All non-hydrogen atoms were made anisotropic, while the hydrogen atoms in **1** were neither detected nor assigned. In **1** atoms C3, O1 and N5 were refined at half occupancy due to the disorder over the mirror plane, and O1 and N5 were constrained to have identical $x$, $y$, $z$ and $U_{ij}$ parameters. The structure of **1** was also solved in P1, which indicated that the disorder was present even in the absence of any crystallographically imposed symmetry.

Crystallographic data (excluding structure factors) for the structures reported in this paper have been deposited with the Cambridge Crystallographic Data Centre as supplementary publication no. CCDC 138773 (**1**), CCDC 138774 (**2**), CCDC 138775 (**4** at 123 K) and CCDC 138776 (**4** at 297 K). Copies of the data can be obtained free of charge on application to CCDC, 12 Union Road, Cambridge CB2 1EZ, UK (fax: (+44) 1223-336-033; e-mail: deposit@ccdc.cam.ac.uk).

**Magnetic studies:** Details of the measurements of DC susceptibilities and magnetisations using a Quantum Design MPMS 5 SQUID magnetometer have been given previously.[6d] The AC susceptibilities were measured with a Quantum Design Physical Property Measurement System (PPMS-7) fitted with an Option P-500 (ACMS) for AC measurements. Samples of about 20 mg were contained in gelatine capsules held at the end of a drinking straw, which was fixed to the sample rod. The AC field used was 3.5 Oe oscillating at 20 Hz.

## Acknowledgement

This work was supported by grants from the Australian Research Council (ARC Large and Small Grants) to KSM. The receipt of an ARC Postdoctoral Fellowship (to SRB) is gratefully acknowledged.

[1] *Molecular Catenanes, Rotaxanes and Knots, A Journey Through the World of Molecular Topology* (Eds.: J.-P. Sauvage, C. Dietrich-Buchecker), Wiley-VCH, Weinheim, **1999**.

[2] S. R. Batten, R. Robson, *Angew. Chem.* **1998**, *110*, 1558; *Angew. Chem. Int. Ed.* **1998**, *37*, 1460.

[3] S. R. Batten, R. Robson, in *Molecular Catenanes, Rotaxanes and Knots, A Journey Through the World of Molecular Topology* (Eds.: J.-P. Sauvage, C. Dietrich-Buchecker), Wiley-VCH, Weinheim, **1999**, pp. 77–105.

[4] B. F. Abrahams, S. R. Batten, M. J. Grannas, H. Hamit, B. F. Hoskins, R. Robson, *Angew. Chem.* **1999**, *111*, 1538; *Angew. Chem. Int. Ed.* **1999**, *38*, 1475.

[5] a) S. R. Batten, B. F. Hoskins, R. Robson, *J. Chem. Soc. Chem. Commun.* **1991**, 445; b) R. Robson, B. F. Abrahams, S. R. Batten, R. W. Gable, B. F. Hoskins, J. Liu, in *Supramolecular Architecture: Synthetic Control in Thin Films and Solids* (Ed.: T. Bein), *ACS Symp. Ser.* **1992**, *499*, 256; c) S. R. Batten, B. F. Hoskins, B. Moubaraki, K. S. Murray, R. Robson, *J. Chem. Soc. Dalton Trans.* **1999**, 2977; d) J. L. Manson, C. Campana, J. S. Miller, *Chem. Commun.* **1998**, 251; e) H. Hoshino, K. Iida, T. Kawamoto, T. Mori, *Inorg. Chem.* **1999**, *38*, 4229.

[6] a) S. R. Batten, P. Jensen, B. Moubaraki, K. S. Murray, R. Robson, *Chem. Commun.* **1998**, 439; b) K. S. Murray, S. R. Batten, B. Moubaraki, D. J. Price, R. Robson, *Mol. Cryst. Liq. Cryst.* **1999**, *335*, 313; c) P. Jensen, S. R. Batten, G. D. Fallon, B. Moubaraki, K. S. Murray, D. J. Price, *Chem Commun.* **1999**, 177; d) S. R. Batten, P. Jensen, C. J. Kepert, M. Kurmoo, B. Moubaraki, K. S. Murray, D. J. Price, *J. Chem. Soc. Dalton Trans.* **1999**, 2987; e) J. L. Manson, C. R. Kmety, Q.-Z. Huang, J. W. Lynn, G. M. Bendele, S. Pagola, P. W. Stephens, L. M. Liable-Sands, A. L. Rheingold, A. J. Epstein, J. S. Miller, *Chem. Mater.* **1998**, *10*, 2552; f) J. L. Manson, C. R. Kmety, A. J. Epstein, J. S. Miller, *Inorg. Chem.* **1999**, *38*, 2552; g) C. R. Kmety, J. L. Manson, Q.-Z. Huang, J. W. Lynn, R. W. Erwin, J. S. Miller, A. J. Epstein, *Phys. Rev. B* **1999**, *60*, 60; h) M. Kurmoo, C. J. Kepert, *New J. Chem.* **1998**, *22*, 1515; i) C. R. Kmety, J. L. Manson, Q.-Z. Huang, J. W. Lynn, R. W. Erwin, J. S. Miller, A. J. Epstein, *Mol. Cryst. Liq. Cryst.* **1999**, *334*, 631; j) M. Kurmoo, C. J. Kepert, *Mol. Cryst. Liq. Cryst.* **1999**, *334*, 693.

[7] a) S. R. Batten, B. F. Hoskins, R. Robson, *Angew. Chem.* **1997**, *109*, 652; *Angew. Chem. Int. Ed. Engl.* **1997**, *36*, 636; b) S. R. Batten, B. F. Hoskins, R. Robson, *New J. Chem.* **1998**, *22*, 173; c) S. R. Batten, B. F. Hoskins, R. Robson, *Inorg. Chem.* **1998**, *37*, 3432; d) S. R. Batten, B. F. Hoskins, R. Robson, *Chem. Eur. J.* **2000**, *6*, 156; e) J. Konnert, D. Britton, *Inorg. Chem.* **1966**, *5*, 1193; f) J. Kozisek, M. Hvastijova, J. Kohout, J. Mrozinski, H. Kohler, *J. Chem. Soc. Dalton Trans.* **1991**, 1773; g) Y. M. Chow, D. Britton, *Acta Crystallogr. Sect. B* **1975**, *31*, 1934; h) K. Brodersen, J. Hofmann, *Z. Anorg. Allg. Chem.* **1992**, *609*, 29; d) D. Britton, Y. M. Chow, *Acta Crystallogr. Sect. C* **1983**, *39*, 1539; i) M. Hvastijova, J. Kohout, J. Kozisek, J. G. Diaz, L. Jager, J. Mrozinski, *Z. Anorg. Allg. Chem.* **1998**, *624*, 349; j) J. Kohout, J. Mrozinski, M. Hvastijova, *Z. Phys. Chem.* **1989**, *270*, 975; k) J. Mrozinski, J. Kohout, M. Hvastijova, *Polyhedron* **1989**, *8*, 157; l) M. Hvastijova, J. Kohout, J. Mrozinski, L. Jager, *Polish J. Chem.* **1995**, *69*, 852.

[8] a) P. Jensen, S. R. Batten, G. D. Fallon, D. C. R. Hockless, B. Moubaraki, K. S. Murray, R. Robson, *J. Solid State Chem.* **1999**, *145*, 387; b) P. Jensen, S. R. Batten, B. Moubaraki, K. S. Murray, *Chem. Commun.* **2000**, 793; c) J. L. Manson, C. D. Incarvito, A. L. Rheingold, J. S. Miller, *J. Chem. Soc. Dalton Trans.* **1998**, 3705; d) J. L. Manson, D. W. Lee, A. L. Rheingold, J. S. Miller, *Inorg. Chem.* **1998**, *37*, 5966; e) J. L. Manson, A. M. Arif, J. S. Miller, *J. Mater. Chem.* **1999**, *9*, 979; f) J. L. Manson, A. M. Arif, C. D. Incarvito, L. M. Liable-Sands, A. L. Rheingold, J. S. Miller, *J. Solid State Chem.* **1999**, *145*, 369; g) J. L. Manson, C. D. Incarvito, A. M. Arif, A. L. Rheingold, J. S. Miller, *Mol. Cryst. Liq. Cryst.* **1999**, *334*, 605; h) D. Britton, Y. M. Chow, *Acta Crystallogr. Sect. B* **1977**, *33*, 697; i) T. Komatsu, H. Sato, T. Nakamura, N. Matsukawa, H. Yamochi, G. Saito, M. Kusunoki, K. Sakaguchi, S. Kagoshima, *Bull. Chem. Soc. Jpn.* **1995**, *68*, 2233.

[9] For other structures with rutile nets, see ref. [7c]; R.-G. Xiong, S. R. Wilson, W. Lin, *J. Chem. Soc. Dalton Trans.* **1998**, 4089.

[10] B. F. Abrahams, M. J. Hardie, B. F. Hoskins, R. Robson, E. E. Sutherland, *J. Chem. Soc. Chem. Commun.* **1994**, 1049.

  0947-6539/00/0617-3194 $ 17.50+.50/0 

[11] S. R. Batten, B. F. Hoskins, R. Robson, *Angew. Chem.* **1995**, *107*, 884; *Angew. Chem. Int. Ed. Engl.* **1995**, *34*, 820.
[12] a) S. J. Rettig, A. Storr, D. A. Summers, R. C. Thompson, J. Trotter, *J. Am. Chem. Soc.* **1997**, *119*, 8675; b) S. J. Rettig, R. C. Thompson, J. Trotter, S. Xia, *Inorg. Chem.* **1999**, *38*, 1360.
[13] O. Kahn, *Molecular Magnetism*, VCH, New York, **1993**, p. 322.
[14] C. Bellitto, F. Federici, S. A. Ibrahim, *Chem. Mater.* **1998**, *10*, 1076.
[15] S. G. Carling, P. Day, D. Visser, R. K. Kremer, *J. Solid State Chem.* **1993**, *106*, 111.
[16] R. L. Carlin, A. J. van Duyneveldt, *Magnetic Properties of Transition Metal Compounds*, Springer, Berlin, **1977**, p. 184.
[17] G. S. Rushbrooke, P. J. Wood, *Mol. Phys.* **1963**, *6*, 409.
[18] M. G. F. Vaz, L. M. M. Pinheiro, H. O. Stumpf, A. F. C. Alcantara, S. Golhen, L. Ouahab, O. Cador, C. Mathoniere, O. Kahn, *Chem. Eur. J.* **1999**, *5*, 1486.
[19] a) M. Kurmoo, *Chem. Mater.*, in press; b) M. Kurmoo, private communication on layered $Co^{II}$ hydroxides, November **1999**.
[20] F. Lloret, G. De Munno, M. Julve, J. Cano, R. Ruiz, A. Caneschi, *Angew. Chem.* **1998**, *110*, 143; *Angew. Chem. Int. Ed.* **1998**, *37*, 135.
[21] P. M. van der Werff, S. R. Batten, P. Jensen, B. Moubaraki, K. S. Murray, unpublished results.
[22] a) C. Mathoniere, C. T. Nuttall, S. G. Carling, P. Day, *Inorg. Chem.* **1996**, *35*, 1201; b) C. J. Nuttall, P. Day, *Chem. Mater.* **1998**, *10*, 3050.
[23] Z. Otwinowski, W. Minor in *Methods in Enzymology* (Eds.: C. W. Carter, R. M. Sweet), Academic Press, New York, **1996**.
[24] G. M. Sheldrick, *SHELX-97, Program for crystal structure refinement*, University of Göttingen, **1997**.
[25] *teXsan: Single Crystal Structure Analysis Software, Version 1.6*, Molecular Structure Corporation, The Woodlands, TX 77381, **1993**.

Received: February 3, 2000 [F2279]